# Interfacial Debonding Mechanism Influenced by Flexural Cracks in FRP-strengthened Beams

Hedong NIU* and Zhishen WU**

*Dr. Candidate of Eng., Dept. of Urban & Civil Eng., Ibaraki Univ., Nakanarusawa-cho 4-12-1, Hitachi Ibaraki 316-8511
**Dr. of Eng., Assoc. Prof., Dept. of Urban & Civil Eng., Ibaraki Univ., Nakanarusawa-cho 4-12-1, Hitachi Ibaraki 316-8511

A sound understanding of the interfacial bonding behavior is of great importance to effective application of fiber reinforced polymers (FRP) to concrete structures. This study mainly focuses on clarifying the fracture and failure mechanisms of FRP debonding due to flexural cracks of concrete in a FRP-strengthened beam. A bilinear shear stress-slip model with softening behavior is adopted to simulate the shear transfer along the FRP-concrete interface. The validity of the theoretical derivations based on theory of linear elasticity is confirmed by comparing the predicted results with both finite element analysis and experimental results. The effect of crack spacing on retrofitted system and debonding mechanism is discussed in detail. According to the theoretical analyses and the authors' previous work, a qualitative criterion governing the onset of debonding (microscopic debonding) and the complete debonding (macroscopic debonding) for the retrofitted beams is clearly established, which can be included in the design guideline for the structural retrofitting with FRP sheets.

***Key Words:*** *fiber reinforced polymers (FRP), flexural crack, debonding, interfacial shear stress, local bond strength, interfacial fracture energy*

## 1. Introduction

The recent earthquakes, such as the 1994 Northridge and 1995 Hyogo-ken Nanbu earthquakes, have repeatedly demonstrated the vulnerabilities of the aged or deteriorated structures to seismic demands. The need to rehabilitate or retrofit the deteriorated civil infrastructure is becoming a major and urgent problem facing the world. In contrast with the traditional structural rehabilitation methods such as introducing additional beams and externally bonded steel plates, the use of fiber reinforced polymers (FRP) as externally bonded reinforcement has gained widespread acceptance as an excellent method for the maintenance, rehabilitation and upgrading of existing concrete structures, which is due to the fact that FRP has much more beneficial characteristics such as high strength- and stiffness-to-weight ratio, high corrosion resistance, electromagnetic neutrality, inherent tailorability and ease of application in the field. Many studies[1), 2), 3), 4)] have showed that significant increases in stiffness, strength and seismic capacities can be achieved by this technique. But recent studies have also observed a wide variety of failure modes, which may limit these gains, such as crushing of concrete, shear failure, FRP rupture, and peeling-off or debonding of FRP at the adhesive-concrete interface. Among these failure modes, the first three modes of failure can be avoided in the structural design and their corresponding ultimate strength of the structural member can be predicted using conventional RC flexural theory. Peeling-off or debonding of FRP from the concrete surface, however, is a new typical failure mode for the retrofitted system and yet little is known about the fracture processes and characteristics of these mechanisms.

The performance of FRP-concrete interface plays a great role in achieving a composite action between concrete and FRP. Fracturing in this region may result in brittle bond failure, involving peeling-off and debonding of FRP due to stress concentrations or bond imperfection, and often significantly lowers the theoretically expected load-carrying capacity of the retrofitted system. Thus there poses an urgent need for a sound understanding of the bond failure

mechanism.

In this paper, we focus on developing a sound understanding of the interfacial bonding behavior and the debonding mechanism in FRP-strengthened R/C beams. According to the beam theory, derivations for bilinear shear-slip model are presented to calculate the interfacial shear stresses and axial forces of FRP due to flexural cracks of concrete. The validity of them is confirmed by comparing the predicted results with both FEM analysis and experimental results. The debonding propagation, the corresponding response of the retrofitted beam and the effect of crack spacing on the debonding mechanism are discussed in detail by combining theoretical analyses with FEM results. Finally, a qualitative criterion governing the onset of debonding (microscopic debonding) and the complete debonding (macroscopic debonding) for the retrofitted beams is clearly established, which can be included in the design guideline for structural retrofitting practices.

## 2. Literature Review

Recently, many studies have been carried out to investigate the bonding and debonding mechanism of pure shear test of FRP[5), 6), 7)]. Kamiharako et al.[5)] proposed a simple bilinear shear stress-slip model for interfacial zone of continuous fiber sheet and concrete based on the uniaxial test to simulate the deformation and peeling-off behavior of continuous fiber sheet. Yuan et al.[6)] introduced varieties of nonlinear interfacial constitutive laws to solve the nonlinear interfacial stress transfer problems for adhesive bonded joint, and derived the corresponding expressions for bonding capacity, interfacial shear stress distribution, initiation and propagation of interfacial crack. Yoshizawa et al.[7)] performed an experimental program of the shear-bonded test between the continuous fiber sheet and concrete. The interfacial fracture energies and the relationship between the local shear stress and relative shear displacement along the CFS-concrete interface were identified. The interfacial local shear stress distribution, effective bonding length, and initiation and propagation of interfacial crack could be well described by using the linearly ascending and descending branch of interfacial stress-slip relationship.

As for the steel/FRP-strengthened beams, considerable researches have been directed to investigate the phenomenon of shear and normal stress concentration at the cut-off point of the FRP plates, and the corresponding failure criteria have been developed for predicting the premature failure load (Roberts[8)], Ziraba et al.[9)], Täljsten[10)], Malek et al.[11)], El-Mihilmy[12)]). The peeling-off initiated from shear cracks of concrete can be prevented by a rational design and much research work on this area has been done[12)]. However, very limited literatures concerning the debonding due to flexural cracks of concrete in the maximum moment region can be found, which is considered to be a more dominant failure mode than the delamination induced by the stress concentrations at curtailment zone for the strengthened beam with FRP sheets. Wu and Niu[13), 14)] adopted linear shear stress-slip model to investigate the effects of flexural cracks on the interfacial shear stresses for several load cases based on linear elastic beam theory and developed an energy-based methodology to predict debonding initiation and final debonding failure of the retrofitted beam. It should be addressed here that linear model cannot locate the true interfacial shear stress at debonding initiation and final debonding failure due to its inherent deficiency. Considering that the bilinear shear stress-slip model can improve the knowledge of debonding failure process, we present a closed-form analytical solution for clarifying the debonding mechanism due to flexural cracks by using the bilinear model and develop a sound methodology to evaluate/design FRP-strengthened R/C beams.

## 3. Theoretical Derivation

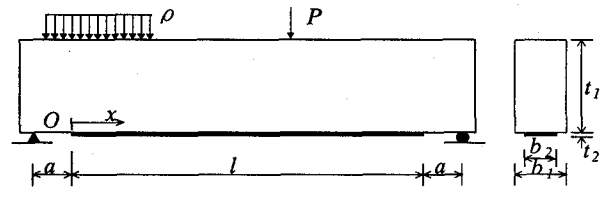


Fig. 1 Simply supported beam strengthened with FRP

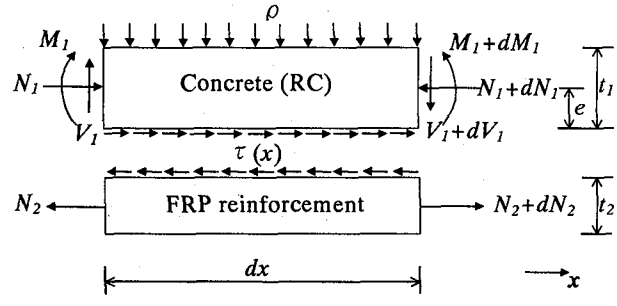


Fig. 2 Forces in infinitesimal element of composite beam

In the present analysis, the following assumptions are made for simplicity of theoretical derivation:

(a) All the materials (R/C and FRP) are regarded to be homogeneous and linear elastic;

(b) The adhesive layer is assumed to only play a role in transferring the stresses from the above concrete to FRP and its thickness can be negligible;

(c) The bending stiffness of FRP is far less than that of the beam to be strengthened and the bending moment

in FRP can be neglected;

(d) Plane section assumption holds for the FRP-strengthened beams.

### 3.1 Basic equations

**(1) Basic equations of elasticity**

On the basis of the assumptions, a differential section, $dx$, can be cut out from the FRP-strengthened R/C beam as shown in Fig. 2 and the basic equations of elasticity can be obtained in what follows.

The strains in concrete (or RC) and FRP near the interface can be expressed by the following equations, respectively:

$$\varepsilon_1(x)=\frac{du_1(x)}{dx}=\frac{M_1(x)}{E_1W_1}-\frac{N_1(x)}{E_1A_1} \tag{1}$$

$$\varepsilon_2(x)=\frac{du_2(x)}{dx}=\frac{N_2(x)}{E_2A_2} \tag{2}$$

The equilibrium conditions of concrete (or RC) in the $x$-direction and moment equilibrium gives:

$x$-direction: $$\frac{dN_1(x)}{dx}=\tau(x)b_2 \tag{3}$$

moment equilibrium: $$\frac{dM_1(x)}{dx}=V_1(x)-\tau(x)b_2e \tag{4}$$

The equilibrium of FRP also gives:

$$\frac{dN_2(x)}{dx}=\tau(x)b_2 \tag{5}$$

**(2) Bilinear stress-slip model**

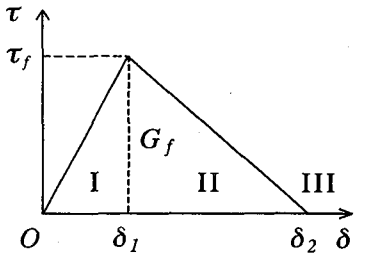


Fig. 3 Bilinear shear stress-slip model

According to the experimental results[5), 7)], a bilinear shear stress-slip model consisting of linearly ascending and descending branch is adopted to give a clear insight into the debonding mechanism in the present study. As shown in Fig. 3, section I, II and III indicate ascending, descending and debonding branch, respectively, and $\tau_f$ is local bond strength, the area below the shear stress-slip curve is interfacial fracture energy $G_f$. The corresponding interfacial shear stress to section I, II and III can be expressed as follows:

$$\tau(\delta)=\begin{cases}\dfrac{\tau_f}{\delta_1}\delta & 0\le\delta\le\delta_1\\ \dfrac{\tau_f}{(\delta_2-\delta_1)}(\delta_2-\delta) & \delta_1<\delta\le\delta_2\\ 0 & \delta_2<\delta\end{cases}$$

$$\delta=u_2(x)-u_1(x) \tag{6}$$

### 3.2 Interfacial shear stresses due to a flexural crack

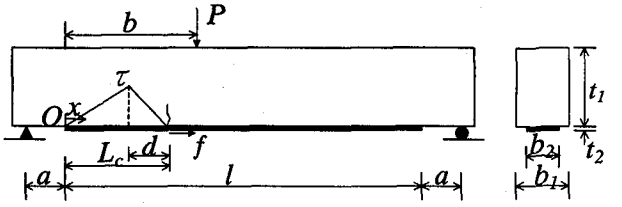


Fig. 4 Three-point bending with a flexural crack

**(1) Linearly ascending branch**

According to equation (6), interfacial shear stress can be expressed as:

$$\tau(x)=\frac{\tau_f}{\delta_1}\left[u_2(x)-u_1(x)\right] \qquad x\in[0,L_c-d] \tag{7}$$

Differentiating equations (7), (1) and (2) respectively with respect to $x$ yields:

$$\frac{d\tau(x)}{dx}=\frac{\tau_f}{\delta_1}\left[\frac{N_2(x)}{E_2A_2}+\frac{N_1(x)}{E_1A_1}-\frac{M_1(x)}{E_1W_1}\right] \tag{8}$$

$$\frac{d^2\tau(x)}{dx^2}=\frac{\tau_f}{\delta_1}\left[\frac{d^2u_2(x)}{dx^2}-\frac{d^2u_1(x)}{dx^2}\right] \tag{9}$$

where $\dfrac{d^2u_1(x)}{dx^2}=\dfrac{1}{E_1W_1}\dfrac{dM_1(x)}{dx}-\dfrac{1}{E_1A_1}\dfrac{dN_1(x)}{dx}$;

$$\frac{d^2u_2(x)}{dx^2}=\frac{1}{E_2A_2}\frac{dN_2(x)}{dx}.$$

Substituting equations (3), (4) and (5) into equation (9) gives:

$$\frac{d^2\tau(x)}{dx^2}-\alpha_1^2\tau(x)+\frac{\tau_f}{E_1W_1\delta_1}V_1(x)=0 \tag{10}$$

where $\alpha_1^2=\dfrac{\tau_f b_2}{\delta_1}\left[\dfrac{1}{E_2A_2}+\dfrac{1}{E_1A_1}+\dfrac{e}{E_1W_1}\right]$; $V_1(x)$ is shear force at section $x$ due to externally applied loads since the shear force in FRP is neglected.

The solution to equation (10) is given by:

$$\tau^{I}(x) = C_1 \cosh(\alpha_1 x) + C_2 \sinh(\alpha_1 x) + \frac{\tau_f}{\alpha_1^2 \delta_1 E_1 W_1} V_1(x) \quad (11)$$

where $C_1$ and $C_2$ are integration constants to be determined by the boundary conditions.

Integrating equation (4) with respect to $x$ with the substitution of equation (5) yields:

$$M_1(x) = M(x) - N_2(x)e \quad (12)$$

where $M(x)$ is the bending moment of the composite beam at section $x$.

Moreover, noticing $N_1(x) = N_2(x)$ and substituting equation (12) into (8) give:

$$N_2^{I}(x) = \frac{b_2}{\alpha_1^2}\left[\frac{d\tau^{I}(x)}{dx} + \frac{\tau_f}{\delta_1}\frac{M(x)}{E_1 W_1}\right] \quad (13)$$

**(2) Linearly descending branch**

According to equation (6), interfacial shear stress can be expressed as:

$$\tau(x) = \frac{\tau_f}{\delta_2 - \delta_1}\left[\delta_2 - u_2(x) + u_1(x)\right] \qquad x \in (L_c - d, L_c] \quad (14)$$

Differentiating equations (14), (1) and (2) respectively with respect to $x$ yields:

$$\frac{d\tau(x)}{dx} = -\frac{\tau_f}{\delta_2 - \delta_1}\left[\frac{N_2(x)}{E_2 A_2} + \frac{N_1(x)}{E_1 A_1} - \frac{M_1(x)}{E_1 W_1}\right] \quad (15)$$

$$\frac{d^2\tau(x)}{dx^2} = -\frac{\tau_f}{\delta_2 - \delta_1}\left[\frac{d^2 u_2(x)}{dx^2} - \frac{d^2 u_1(x)}{dx^2}\right] \quad (16)$$

Substituting equations (3), (4) and (5) into equation (16) gives:

$$\frac{d^2\tau(x)}{dx^2} + \alpha_2^2 \tau(x) - \frac{\tau_f V_1(x)}{E_1 W_1(\delta_2 - \delta_1)} = 0 \quad (17)$$

where $\alpha_2^2 = \frac{\tau_f b_2}{\delta_2 - \delta_1}\left[\frac{1}{E_2 A_2} + \frac{1}{E_1 A_1} + \frac{e}{E_1 W_1}\right]$.

The solution to equation (17) is given by:

$$\tau^{II}(x) = C_3 \sin\left[\alpha_2(x - L_c + d)\right] + C_4 \cos\left[\alpha_2(x - L_c + d)\right] + \frac{\tau_f V_1(x)}{\alpha_2^2(\delta_2 - \delta_1)E_1 W_1} \quad (18)$$

where $C_3$ and $C_4$ are integration constants to be determined by the boundary conditions.

Similarly, the axial force of FRP in the softening branch can be expressed as:

$$N_2^{II}(x) = \frac{b_2}{\alpha_2^2}\left[-\frac{d\tau(x)}{dx} + \frac{\tau_f}{(\delta_2 - \delta_1)}\frac{M(x)}{E_1 W_1} + \frac{\tau_f}{(\delta_2 - \delta_1)}\frac{N_2^{I}(L_c - d)e}{E_1 W_1}\right] \quad (19)$$

**(3) Determination of integration constants**

Case 1: The shear stress state is only located in ascending branch, which can be referred to Wu and Niu [13][14].

$$C_1 = \frac{\frac{\tau_f}{\delta_1 \alpha_1 E_1 W_1}\left\{a\left[\cosh(\alpha_1 L_c) - 1\right] - L_c\right\}V_1(x) + \frac{\alpha_1 f}{b_2}}{\sinh(\alpha L_c)}$$

$$C_2 = -\frac{\tau_f V_1(x) a}{\delta_1 \alpha_1 E_1 W_1} \quad (20)$$

Case 2: The shear stress state enters the softening branch.

As shown in Fig. 4, the boundary conditions can be expressed as:

$$\begin{cases} N_2^{I}(x) = 0 & x = 0 \\ N_2^{I}(x) = N_2^{II}(x) & x = L_c - d \\ \tau^{I}(x) = \tau_f & x = L_c - d \\ \tau^{II}(x) = \tau_f & x = L_c - d \\ N_2^{II}(x) = f & x = L_c \end{cases} \quad (21)$$

Substituting equations (11), (13), (18) and (19) into the above expressions gives:

$$C_1 = \frac{\tau_f + \frac{\tau_f V_1(x)}{\alpha_1^2 \delta_1 E_1 W_1}\left\{\alpha_1 a \sinh\left[\alpha_1(L_c - d)\right] - 1\right\}}{\cosh\left[\alpha_1(L_c - d)\right]}$$

$$C_2 = -\frac{\tau_f V_1(x) a}{\alpha_1 \delta_1 E_1 W_1}$$

$$C_3 = -\frac{\alpha_2}{\alpha_1}\left\{\left[\tau_f - \frac{\tau_f V_1(x)}{\alpha_1^2 \delta_1 E_1 W_1}\right]\tanh\left[\alpha_1(L_c - d)\right] - \frac{1}{\cosh\left[\alpha_1(L_c - d)\right]}\frac{\tau_f V_1(x) a}{\alpha_1 \delta_1 E_1 W_1}\right\} + \left[\frac{\tau_f}{\alpha_2(\delta_2 - \delta_1)} - \frac{\alpha_2 \tau_f}{\alpha_1^2 \delta_1}\right]\frac{V_1(x)(L_c - d + a)}{E_1 W_1}$$

$$C_4 = \tau_f - \frac{\tau_f V_1(x)}{\alpha_2^2(\delta_2 - \delta_1)E_1 W_1} \quad (22)$$

$$b_2\left\{\frac{1}{\alpha_2}\left[C_4\sin(\alpha_2 d)-C_3\cos(\alpha_2 d)\right]+\frac{\tau_f}{\alpha_2^2(\delta_2-\delta_1)}\frac{V_1(x)(L_c+a)}{E_1W_1}\right\}=f \tag{23}$$

The length of descending branch, $d$, can be calculated by equation (23) and then the interfacial shear stress distribution can be obtained according to equations (11), (18) and (22).

### 3.3 Interfacial shear stresses between two flexural cracks

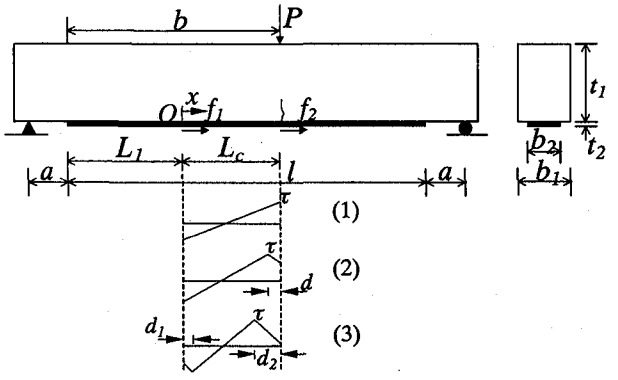


Fig. 5 Three-point bending beam with two flexural cracks

Considering that the shear stresses distributed in $L_1$ segment can be obtained by the aforementioned equations, the shear stresses between two flexural cracks are derived for three cases in this section.

**(1) Case 1: The shear stress state is only located in ascending branch, which can be referred to Wu and Niu [14]**

$$C_2=\frac{\alpha_1 f_1}{b_2}-\frac{\tau_f V(x)(a+L_1)}{\alpha_1\delta_1 E_1W_1}$$

$$C_1=\frac{\dfrac{\alpha_1 f_2}{b_2}-\dfrac{\tau_f V_1(x)(a+L_1+L_c)}{\alpha_1\delta_1 E_1W_1}-C_2\cosh(\alpha_1 L_c)}{\sinh(\alpha_1 L_c)} \tag{24}$$

**(2) Case 2: Only the shear stress state at the end of the crack located at larger moment region enters softening branch**

As shown in Fig. 5, the boundary conditions can be expressed as follows:

$$\begin{cases} N_2^I(x)=f_1 & x=0\\ N_2^I(x)=N_2^{II}(x) & x=L_c-d\\ \tau^I(x)=\tau_f & x=L_c-d\\ \tau^{II}(x)=\tau_f & x=L_c-d\\ N_2^{II}(x)=f_2 & x=L_c \end{cases} \tag{25}$$

Substituting equations (11), (13), (18) and (19) into the above expressions gives:

$$C_2=\frac{\alpha_1 f_1}{b_2}-\frac{\tau_f V_1(x)(a+L_1)}{\alpha_1\delta_1 E_1W_1}$$

$$C_1=\frac{\tau_f-C_2\sinh[\alpha_1(L_c-d)]-\dfrac{\tau_f V_1(x)}{\alpha_1^2 E_1W_1}}{\cosh[\alpha_1(L_c-d)]}$$

$$C_3=\frac{\tau_f V_1(x)(a+L_1+L_c-d)}{\alpha_2 E_1W_1(\delta_2-\delta_1)}-\frac{\alpha_2}{\alpha_1}\left\{C_1\sinh[\alpha_1(L_c-d)]+C_2\cosh[\alpha_1(L_c-d)]+\frac{\tau_f V_1(x)(a+L_1+L_c-d)}{\alpha_1\delta_1 E_1W_1}\right\}$$

$$C_4=\tau_f-\frac{\tau_f V_1(x)}{\alpha_2^2 E_1W_1(\delta_2-\delta_1)} \tag{26}$$

$$\frac{b_2}{\alpha_2}\left\{C_4\sin(\alpha_2 d)-C_3\cos(\alpha_2 d)+\frac{\tau_f V_1(x)(a+L_1+L_c)}{\alpha_2 E_1W_1(\delta_2-\delta_1)}\right\}=f_2 \tag{27}$$

The length of descending branch, $d$, can be calculated by equation (27) and then the interfacial shear stress distribution can be obtained according to equations (11), (18) and (26).

**(3) Case 3: The shear stress states at the ends of cracks enter softening branch and others are located in ascending branch**

The expressions for shear stresses and the axial forces of FRP in three parts can be given by:

For the segment $x\in[0,d_1]$:

$$\tau^{II}(x)=C_1\sin(\alpha_2 x)+C_2\cos(\alpha_2 x)+\frac{\tau_f V_1(x)}{\alpha_2^2 E_1W_1(\delta_2-\delta_1)}$$

$$N_2^{II}(x)=\frac{b_2}{\alpha_2}\left\{C_2\sin(\alpha_2 x)-C_1\cos(\alpha_2 x)+\frac{\tau_f M(x)}{\alpha_2 E_1W_1(\delta_2-\delta_1)}\right\}$$

For the segment $x\in(d_1,L_c-d_2]$:

$$\tau^{I}(x)=C_3\cosh[\alpha_1(x-d_1)]+C_4\sinh[\alpha_1(x-d_1)]+\frac{\tau_f V_1(x)}{\alpha_1^2 E_1W_1\delta_1}$$

$$N_2^{I}(x)=\frac{b_2}{\alpha_1}\left\{C_3\sinh[\alpha_1(x-d_1)]+C_4\cosh[\alpha_1(x-d_1)]+\frac{\tau_f M(x)}{\alpha_1\delta_1 E_1W_1}\right\}$$

For the segment $x \in (L_c - d_2, L_c]$:

$$\tau^{II}(x) = C_5 \sin[\alpha_2(x - L_c + d_2)] + C_6 \cos[\alpha_2(x - L_c + d_2)] + \frac{\tau_f V_1(x)}{\alpha_2^2 E_1 W_1(\delta_2 - \delta_1)}$$

$$N_2^{II}(x) = \frac{b_2}{\alpha_2}\left\{C_6 \sin[\alpha_2(x - L_c + d_2)] - C_5 \cos[\alpha_2(x - L_c + d_2)] + \frac{\tau_f M(x)}{\alpha_2 E_1 W_1(\delta_2 - \delta_1)}\right\}$$

The boundary conditions for this case can be expressed as follows:

$$\begin{cases} N_2^{II}(x) = f_1 & x = 0 \\ N_2^{II}(x) = N_2^{I}(x) & x = d_1 \\ \tau^{II}(x) = -\tau_f & x = d_1 \\ \tau^{I}(x) = -\tau_f & x = d_1 \\ \tau^{I}(x) = \tau_f & x = L_c - d_2 \\ \tau^{II}(x) = \tau_f & x = L_c - d_2 \\ N_2^{I}(x) = N_2^{II}(x) & x = L_c - d_2 \\ N_2^{II}(x) = f_2 & x = L_c \end{cases} \tag{28}$$

According to the above expressions for three parts and equation (28), we can obtain the integration constants:

$$C_1 = -\frac{\alpha_2 f_1}{b_2} + \frac{\tau_f V_1(a + L_1)}{\alpha_2 E_1 W_1(\delta_2 - \delta_1)}$$

$$C_2 = -\frac{\tau_f + C_1 \sin(\alpha_2 d_1) + \frac{\tau_f V_1(x)}{\alpha_2^2 E_1 W_1(\delta_2 - \delta_1)}}{\cos(\alpha_2 d_1)}$$

$$C_3 = -\tau_f - \frac{\tau_f V_1(x)}{\alpha_1^2 \delta_1 E_1 W_1}$$

$$C_4 = \frac{\tau_f - \frac{\tau_f V_1(x)}{\alpha_1^2 \delta_1 E_1 W_1} - C_3 \cosh[\alpha_1(L_c - d_1 - d_2)]}{\sinh[\alpha_1(L_c - d_1 - d_2)]}$$

$$C_5 = \frac{\tau_f V_1(x)(a + L_1 + L_c - d_2)}{\alpha_2 E_1 W_1(\delta_2 - \delta_1)} - \frac{\alpha_2}{\alpha_1}\left\{C_3 \sinh[\alpha_1(L_c - d_1 - d_2)] + C_4 \cosh[\alpha_1(L_c - d_1 - d_2)] + \frac{\tau_f V_1(x)(a + L_1 + L_c - d_2)}{\alpha_2 E_1 W_1(\delta_2 - \delta_1)}\right\}$$

$$C_6 = \tau_f - \frac{\tau_f V_1(x)}{\alpha_2^2 E_1 W_1(\delta_2 - \delta_1)} \tag{29}$$

$$\frac{b_2}{\alpha_2}\left\{C_2 \sin(\alpha_2 d_1) - C_1 \cos(\alpha_2 d_1) + \frac{\tau_f V_1(x)(a + L_1 + d_1)}{\alpha_2 E_1 W_1(\delta_2 - \delta_1)}\right\} = \frac{b_2}{\alpha_1}\left[C_4 + \frac{\tau_f V_1(x)(a + L_1 + d_1)}{\alpha_1 \delta_1 E_1 W_1}\right] \tag{30}$$

$$\frac{b_2}{\alpha_2}\left\{C_6 \sin(\alpha_2 d_2) - C_5 \cos(\alpha_2 d_2) + \frac{\tau_f V_1(x)(a + L_1 + L_c)}{\alpha_2 E_1 W_1(\delta_2 - \delta_1)}\right\} = f_2 \tag{31}$$

A trial and error method should be used to determine the lengths of descending branch, $d_1$ and $d_2$, according to equations (30) and (31), and then the interfacial shear stress distribution can be obtained by the above equations.

## 4. Verification of Theoretical Derivations

In order to verify the correctness of the aforementioned equations, the predicted results are compared with both finite element method analysis and experimental results. According to Triantafillou and Plevris[15], debonding often occurs when the peak value of the interface shear stress reaches a limiting value which depends on the strength of concrete and this limit value is approximately 8MPa for normal-strength concrete. In addition, Yoshizawa et al.[7] have identified the bilinear shear stress-slip curve from the experiments: $\delta_1 = 0.05$mm, $\delta_2 = 0.3$mm and $\tau_f = 8$MPa, which is adopted in the following analysis.

### 4.1 Comparison with finite element analysis

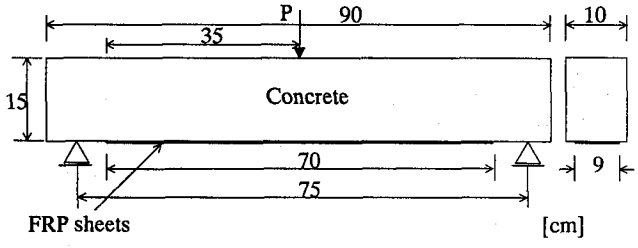


Fig. 6 A FRP-strengthened beam used in FEM analysis

Table 1 Material properties for the studied specimen

| | | |
|---|---|---|
| Concrete | Young's modulus [GPa] | 30 |
| | Compressive strength [MPa] | 39.2 |
| | Poisson's ratio | 0.16 |
| CFRP sheets | Young's modulus [GPa] | 235 |
| | Tensile strength [GPa] | 3.2 |
| | Thickness [mm] | 0.11 |
| | Poisson's ratio | 0.3 |

A FRP-strengthened beam shown in Fig. 6 is analyzed with the derived equations and the "ABAQUS" finite element program (ABAQUS, Version 5.8, 1998). The material properties are listed in Table 1.

**(1) Structural modeling**

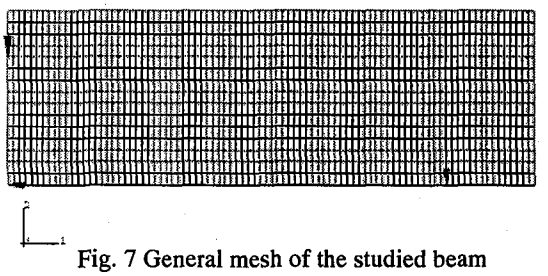

Fig. 7 General mesh of the studied beam

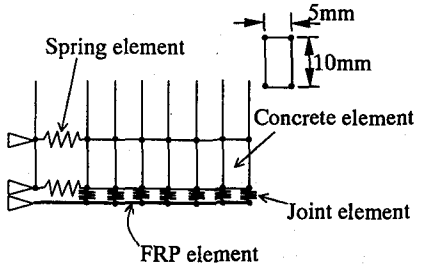


Fig. 8 Detailed mesh definition and material models

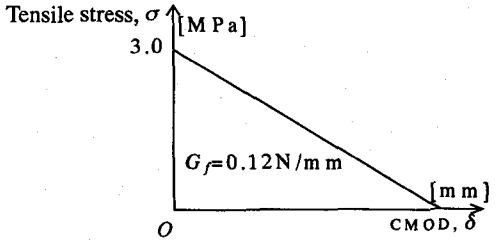


Fig. 9 A tension-softening model used to simulate the behavior of crack

Due to the symmetry of the composite beam, only half of the beam is analyzed with appropriate constraints at the centerline, as shown in Fig. 7. The concrete beam is modeled by 4-node plane stress elements (CPS4) and FRP is modeled by 2-node linear truss elements (T2D2). The flexible joint elements (JOINTC) are used to model the behavior of interface, where the shear stress-slip curve can be defined by nonlinear spring behavior. In order to simulate the initiation and propagation of flexural crack, spring elements (SPRING2) are adopted along the whole central section of the beam. The spring element theoretically should have an infinitely great stiffness before onset of crack to keep inner elasticity and after reaching the tensile strength should follow the assumed tension-softening model shown in Fig. 9. All the materials except those of modeling the interface and the flexural crack are assumed to behave in linear elasticity.

**(2) Simulation of response of FRP-strengthened beam**

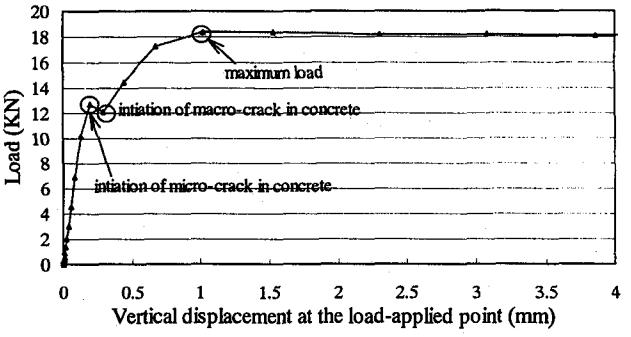


(a) Structural response of the composite beam

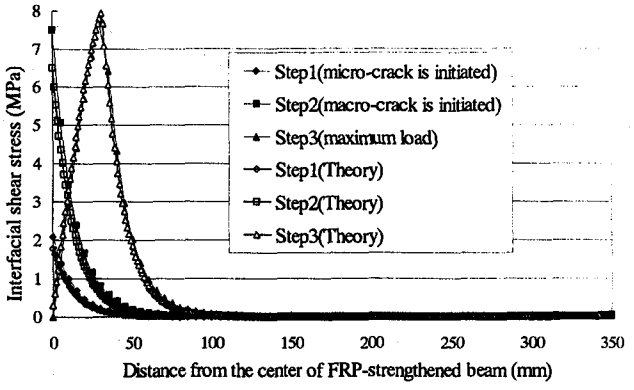


(b) Interfacial shear stress distribution for different stages

Fig. 10 Simulation of FRP-strengthened beam with one flexural crack

First we study the case for FRP-strengthened beam with one unique flexural crack at the center. Fig. 10 (a) shows initiation and propagation of the flexural crack during the loading process. Crack initiation (micro-cracking) and complete crack (macro-cracking) are defined respectively to occur when the tensile stress of concrete reaches its tensile strength and when the fracture energy (i.e. the area below the softening stress-crack mouth opening displacement curve) is reached. As seen from Fig. 10 (b), three stages marked as micro-cracking, macro-cracking and maximum loading are used to compare FEM analysis with the predicted results by theoretical equations and it is found that the theoretical prediction is in a good agreement with the FEM results.

Then the case with multiple cracks is considered to verify the correctness of the closed-form solutions. According to Fig. 10 (b), effective shear transfer length for the present studied beam can be regarded to be about 10cm. So three kinds of crack spacing: 5cm, 10cm and 15cm are modeled to investigate the corresponding shear stress distribution and the structural response. Fig. 11(a) clearly illustrates the deformation of the composite beam with predefined flexural cracks spacing at 10cm. The structural

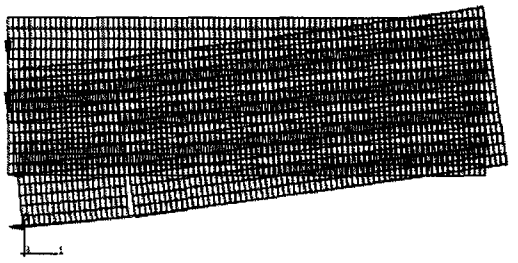

(a) Deformation of 10cm crack spacing case displaced at 5mm

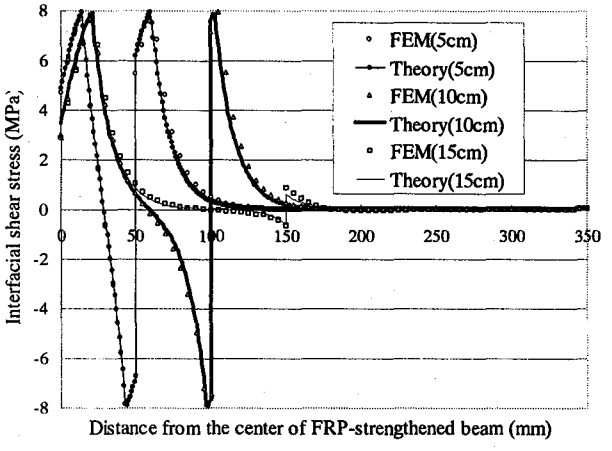


(b) Interfacial shear stress distribution at Load=18KN

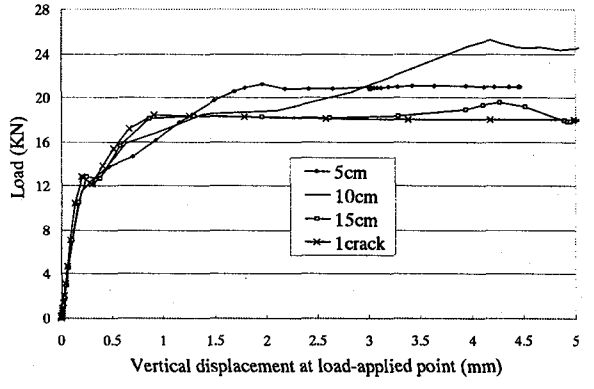


(c) Structural responses for single crack and multiple cracks

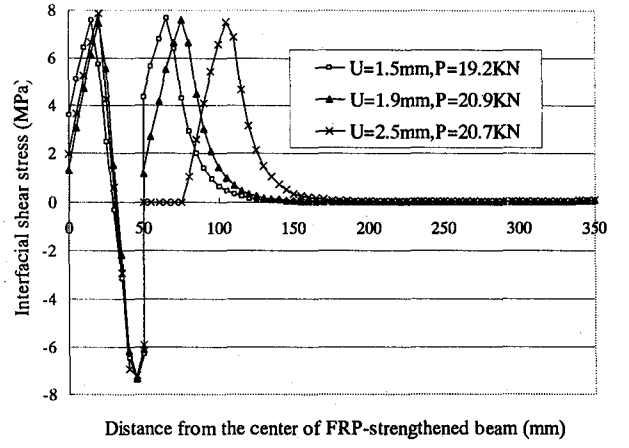


(d) Debonding propagation for 5cm crack spacing case

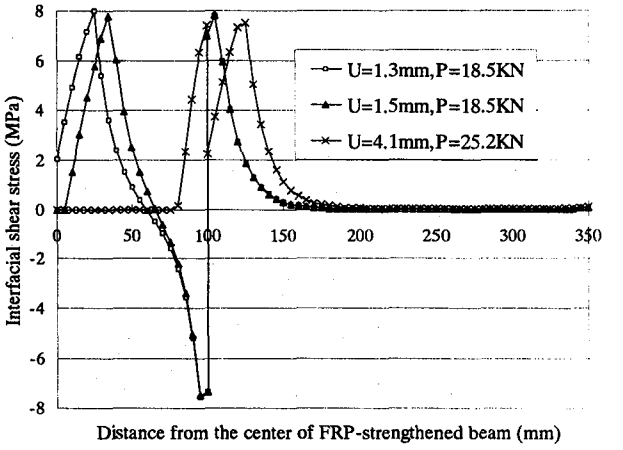


(e) Debonding propagation for 10cm crack spacing case

Fig. 11 Simulation of FRP-strengthened beam with multiple flexural cracks

responses and the propagation of debonding for these three kinds of crack spacing by FEM are illustrated in Fig. 11 (b), (c), (d) and (e). Fig. 11(b) clearly shows that the overall prediction by present method is in a relatively good agreement with the results of FEM simulation and the shear transfer between flexural cracks is significantly affected by crack spacing. Seen from Fig. 11 (c), it is found that crack spacing much lager than the effective transfer length may yield a close load-carrying capacity to one single crack case and the strengthening effect of FRP can be fully utilized only at the crack spacing close to the effective transfer length. The effect of crack spacing on debonding propagation is clearly illustrated in Fig. 11 (d) and (e). It should be pointed out that some fluctuations in FEM analysis should be attributed to the assumption of linear elastic material.

### 4.2 Comparison with experimental results

Kurokawa et al.[16] performed an experimental program to investigate the crack characteristics and the flexural strengthening of CFRP plate-strengthened RC beams. The test beam, as shown in Fig. 12, was provided with 0.11 mm thick CFRP sheet U-shaped end anchorages to prevent the premature delamination at ends of CFPR plate. On the basis of the aforementioned derivations, the interfacial shear stress state can be determined by the measured axial force of FRP near the center of the beam and then the corresponding axial forces can be calculated. The prediction assumes that only one flexural crack occurs at the maximum moment region. In Fig. 13, the predicted axial forces of FRP at pre- and post-cracking stages are compared with the experimental ones in which the data near the center of the beams are not provided because of the strain gauges damaged due to some uncertain factors in test. It can be found that apparent difference lies

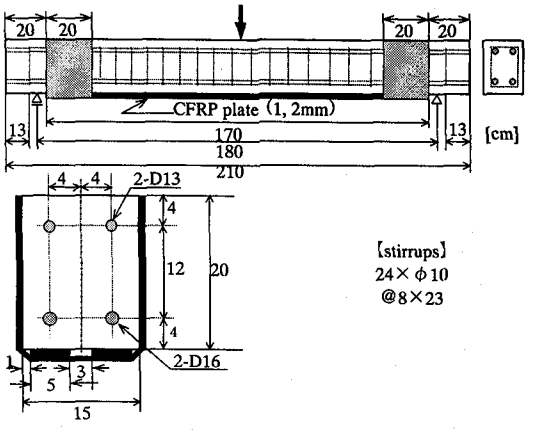


Fig. 12 Details of specimen tested by Kurokawa et al.[16]

Table 2 Material properties for the specimen

| Materials | Properties | Values |
|---|---|---|
| Concrete | Young's modulus | 30.2 (GPa) |
| | Compressive strength | 43.5 (MPa) |
| | Poisson's ratio | 0.13 |
| Reinfocing bar | Young's modulus | 2100 (GPa) |
| | Tensile strength | 420 (MPa) |
| CFRP plate | Design thickness(1mm plate) | 0.6 (mm) |
| | Design thickness(2mm plate) | 1.2 (mm) |
| | Young's modulus | 127.5 (GPa) |
| | Tensile strength | 2.3 (GPa) |
| | Poisson's ratio | 0.3 |

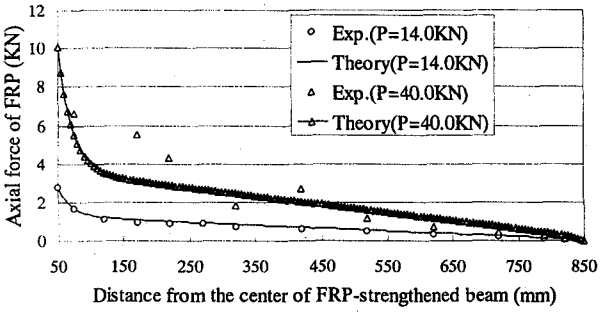


(a) Case for 1mm CFRP plate

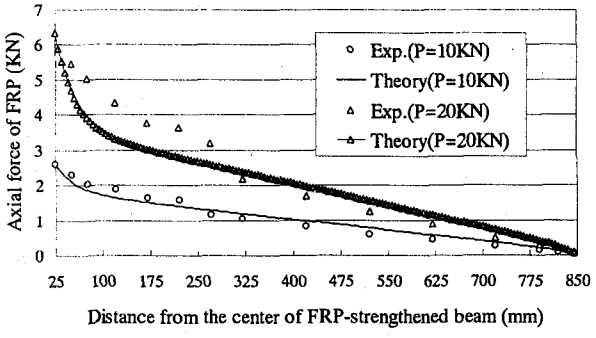


(b) Case for 2mm CFRP plate

Fig. 13 Comparison of the predicted results with experimental ones

between the predicted results and the experimental ones at the post-cracking stage, which can be attributed to the assumption of only one single crack appearing near the maximum moment region. Nevertheless, the overall prediction is in a relatively good agreement with the experimental results.

## 5. Investigation into Debonding Mechanism Influenced by Flexural Cracks of Concrete

### 5.1 Concept of debonding initiation and complete debonding

From an engineer's point of view, it is necessary to establish a simple guideline to design/evaluate FRP-strengthened beams free of debonding due to flexural cracks. In this section, a criterion governing initiation and propagation of debonding is proposed based on the previous works done by the authors[13), 14)].

First we give some clear definitions concerning the present model shown in Fig. 3. When exerting the load on the FRP-strengthened beam, the following stages shown in Fig. 14 appears one by one:

Stage 1: With increase of external load, flexural cracks first occur in the maximum moment region. A large axial force of FRP at flexural crack induces a significant increase in the nearby shear stresses. In this stage, FRP-concrete interface is located in the ascending branch (Section I) and no interfacial debonding occurs. When the maximum shear stress at flexural crack reaches the local bond strength, interfacial debonding is initiated (micro-debonding).

Stage 2: In this stage, FRP-concrete interface is in a complicated state, where some parts enter the softening branch (Section II) and others are located in the ascending branch (Section I). With increase in length of softening zone, the location of maximum shear stress (equal to the local bond strength in value) moves from the flexural crack to the other end of FRP, which can be called propagation of micro-debonding. When loading to a certain value, the slip at flexural crack attains the ultimate tolerant value and the shear stress decrease to zero. At this time, micro-debonding becomes a complete debonding (macro-debonding). In essence, a certain loading value is required to provide sufficient interfacial strain energy release rate so as to reach the interfacial fracture energy consumed for complete debonding and the interfacial fracture energy governs the formation of macro-debonding.

Stage 3: After the formation of complete debonding, the propagation of debonding in this stage may be very unstable and whether or not final debonding failure occurs depends on the flexural crack pattern in concrete, which will be discussed in detail in what follows.

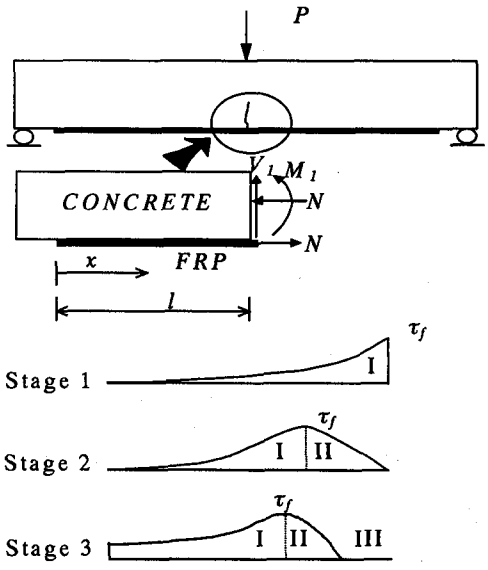


Fig. 14 Different stages illustrating the shear stress distribution

From what stated above, it could be easily concluded that the local bond strength is mainly responsible for the initiation of debonding and the propagation of debonding is governed by the interfacial fracture energy.

### 5.2 Discussions on debonding mechanism according to analysis of FEM and experimental phenomena

Generally, there are two typical flexural crack patterns for final debonding failure observed in the experiment conducted by Wu et al.[3), 4)]: only one mainly centralized flexural crack appearing in FRP-strengthened plain concrete beams and many distributed cracks in FRP-strengthened RC beams. For FRP-strengthened plain concrete beams, once a complete debonding or macro-debonding is initiated, the final debonding failure occurs through the propagation of interfacial crack. But this case does not always hold true for FRP-strengthened RC beams, which can be clearly illustrated in Fig. 10 and Fig. 11.

As for the analysis presented in Fig. 10, a unique flexural crack appears in the composite beam and the maximum load reaches when a complete debonding is exactly initiated. After the formation of macro-debonding, external load keeps nearly constant during the fracture propagation of interfacial crack to the end of FRP sheets. In practice, afterwards load will suddenly drop and final debonding failure will occur. The discrepancy between FEM analysis and experimental observation can be attributed to linear elastic assumption of all the materials in FEM simulation. It is believed that the interfacial shear stress is mainly provided by the axial stress difference in FRP. According to Wu and Niu[14)], the axial force of FRP at a flexural crack is far large than that at the uncracked location very near to the crack. As shown in Fig. 15, for the case of unique or centralized crack, there is no other crack to resist the debonding propagation after the formation of macro-debonding, which can explain why final debonding failure occurs when a complete debonding is initiated.

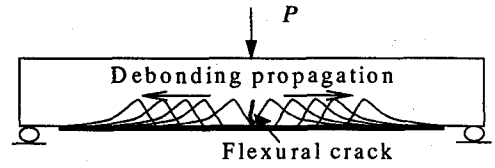


Fig. 15 Debonding mechanism for plain concrete beams strengthened with FRP

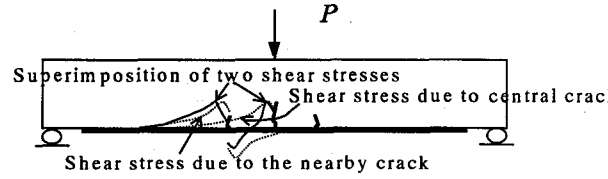


(a) 5cm crack spacing case (<<effective transfer length)

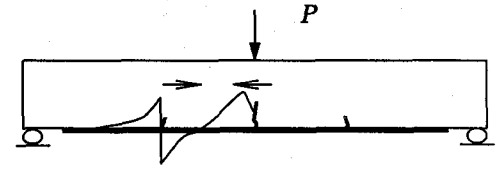


(b) 10cm crack spacing case (≈ effective transfer length)

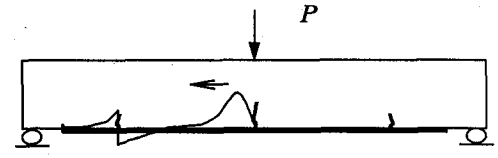


(c) 15cm crack spacing case (>> effective transfer length)

Fig. 16 Debnding mechanism for FRP-strengthened RC beams with multiple cracks

For the case of Fig. 11, there are three cracks used to model final debonding failure for FRP-strengthened RC beam with multiple cracks. It is found that crack spacing affects debonding propagation and the reinforcement effect of FRP. For the case of 5 cm crack spacing, a complete debonding is not initially formed at the central crack. This can be attributed to that crack spacing is much less than effective transfer length and the superimposition effect of two shear stresses near the crack is strengthened, which is clearly shown in Fig. 16 (a). Once a complete debonding is formed external load keeps constant in FEM analysis, which signifies final debonding failure in fact. For the case of 10cm crack spacing, a complete debonding is first formed at central crack. The axial force of FRP at nearby crack significantly increases so as to produce an opposite shear stress to resist the debonding propagation as shown in Fig.16

(b), which lead to continuous increase in external load. When overcoming the resistance and the complete debonding zone reaching the nearby crack, debondng failure occurs. For the case of 15cm crack spacing which is greater than the effective shear transfer length (Fig. 16(c)), the debonding mechanism and the corresponding load-carrying capacity can be regarded to be close to those of unique flexural crack case.

In a summary, a complete debonding can be regarded as necessary and sufficient condition for final debonding failure of FRP-strengthened plain concrete beams. However, it is only a necessary condition for FRP-strengthened RC beams to develop final debonding failure, which indicates that a complete debonding will not result in final debonding failure immediately.

### 5.3 An improved criterion governing initiation of debonding and debonding failure

Wu and Niu[13] proposed an energy-based method for predicting final debonding failure load for FRP-strengthened RC beams, and conducted the identification of maximum shear stresses and interfacial fracture energies consumed for debonding initiation and final debonding failure[13), 14)]. Due to inherent deficiency of linear elastic model, the identified maximum shear stresses are out of range of normal values. Based on those works, an improved design criterion governing debonding initiation and final debonding failure is proposed here:

(1) The present theoretical derivations can be used to identify the local bond strength of FRP-concrete interface in FRP-strengthened beams which determines whether or not debonding is initiated.

(2) The interfacial fracture energy consumed for final debonding failure can be identified by different calculation methods respectively for FRP-strengthened plain concrete beams and FRP-strengthened RC beams. For the case of plain concrete beams, the axial force of FRP at the centralized flexural crack can be used to calculate the interfacial fracture energy. As for the RC beams, the difference of axial force of FRP at the central and nearby crack can be used to identify the fracture energy. The detailed information can be found in Wu and Niu[13].

(3) With these two governing parameters, local bond strength and interfacial fracture energy consumed for final debonding failure, debonding initiation and final debonding failure can be evaluated or avoided in the practical design.

## 6. Conclusions

Up to date, few studies are conducted to investigate the debonding mechanism due to flexural cracks in FRP-strengthened R/C beams. The present study presents closed-form solutions of interfacial shear stress for this failure mode to clarify the initiation and propagation of debonding and confirms the validity of the derivations by comparing the prediction with both FEM analysis and experimental results. Some useful discussions are made and an explicit criterion governing initiation and propagation of debonding is established, which can be included in the design guideline. It is believed that the present analysis can provide a deep insight into understanding of the shear transfer behavior and the debonding mechanism caused by flexural cracks of concrete in the retrofitted concrete beams.

### Appendix Notations

The following symbols are used in this paper:

$A_1$ = cross-sectional area of R/C beam;
$A_2$ = cross-sectional area of FRP;
$a$ = distance between support and end of FRP;
$b$ = distance between load-applied point and end of FRP;
$b_1$ = width of R/C beam;
$b_2$ = width of FRP;
$C_{1\text{-}6}$ = integration constants;
$d$ = softening length;
$d_1$ = softening length near the secondary crack;
$d_2$ = softening length near the first crack;
$e$ = distance from neutral axis to bottom of R/C beam;
$E_1$ = elastic modulus of concrete;
$E_2$ = elastic modulus of FRP;
$f$ = axial force of FRP at crack;
$f_1$ = axial force of FRP at the secondary crack;
$f_2$ = axial force of FRP at the first crack;
$G_f$ = area below the shear stress-slip curve, i.e., the interfacial fracture energy consumed for complete debonding;
$l$ = length of FRP;
$L_1$ = distance between the secondary crack and end of FRP;
$L_c$ = distance between crack and end of FRP for the beam with one flexural crack, and two cracks for the beam with multiple flexural cracks;
$M$ = bending moment of composite beam;
$M_1$ = bending moment of R/C beam;
$N_1$ = axial force of R/C beam;
$N_2$ = axial force of FRP;
$P$ = applied load;
$t_1$ = height of R/C beam;

$t_2$ = thickness of FRP;
$u_1$ = local displacement of R/C beam near the interface along $x$-direction;
$u_2$ = local displacement of FRP near the interface along $x$-direction;
$V_1$ = shear force of R/C beam;
$W_1$ = section modulus of R/C beam;
$x$ = coordinate with reference to the origin;
$\alpha_{1\text{-}2}$ = coefficients used in linearly ascending and descending branches;
$\delta$ = relative slip between R/C beam and FRP at interface;
$\delta_1$ = slip at which shear stress reaches the local bond strength;
$\delta_2$ = slip over which shear stress vanish;
$\varepsilon_1$ = strain in R/C beam near the interface;
$\varepsilon_2$ = strain in FRP near the interface;
$\rho$ = distributed load per unit area on R/C beam;
$\tau$ = interfacial shear stress;
$\tau_f$ = local bond strength;

$^{I}$ and $^{II}$ = indicating ascending and descending branch, respectively.

**References**


1) An, W., Saadatmanesh, H. and Ehsani, M. R., *RC beams strengthened with FRP plates II: Analysis and parametric study*, Journal of Structural Engineering, ASCE, Vol. 117, No. 11, pp.3434-3455, November, 1991
2) Wu, Z. S., *Research trends onretrofitting and strengthening concrete structures by FRP sheets and plates*, International Conference on Fibre Reinforced Concrete, pp.9-17, October, 1997, Guangzhou, China
3) Wu, Z. S., Matsuzaki, T. and Tanabe, K., *Experimental study on fracture mechanism of FRP-reinforced concrete beams*, Symposium on Non-Metallic (FRP) Reinforcement for Concrete Structures, Japan Concrete Institute, pp.119-126, May, 1998 (In Japanese)
4) Wu, Z. S., Matsuzaki, T., Fukuzawa, K. and Kanda, T., *Strengthening effects on RC beams with externally prestressed carbon fiber sheets*, Journal of Materials, Concrete Structures and Pavements, JSCE, Vol. 46, No. 641, pp.153-165, February, 2000 (In Japanese)
5) Kamiharako, A., Shimomura, T., Maruyama, K. and Nishida, H., *Stress transfer and peeling-off behavior of continuous fiber reinforced sheet-concrete system*, The Seventh East Asia-Pacific Conference on Structural Engineering & Construction, pp.1283-1288, August 27-29, 1999, Kochi, Japan
6) Yuan, H., Wu, Z. S. and Yoshizawa, H., *Theoretical solutions on interfacial stress transfer of externally bonded steel/composite laminates,* Journal of Structural Mechanics and Earthquake Engineering, JSCE, 2000 (to appear)
7) Yoshizawa, H., Wu, Z. S., Yuan, H. and Kanakubo, T., *Study on FRP-concrete interface bond performance,* Journal of Materials, Concrete Structures and Pavements, JSCE, Vol. 49, No. 662, pp. 105-119, November, 2000 (In Japanese)
8) Roberts, T. M., *Approximate analysis of shear and normal stress concentrations in the adhesive layer of plated RC beams*, The Structural Engineer, Vol. 67, No. 12, pp.229-233, 20 June, 1989
9) Ziraba, Y. N., Baluch, M. H., Basunbul, I. A., Sharif, A. M., Azad, A. K., and Al-Sulaimani, G. J., *Guidelines toward the design of reinforced concrete beams with external plates*, ACI Structural Journal, Vol. 91, No. 6, pp.639-646, November-December, 1994
10) Täljsten, B., *Strengthening of beams by plate bonding,* Journal of Materials in Civil Engineering, ASCE, Vol. 9, No. 4, pp.206-212, November, 1997
11) Malek, A. M., Saadatmanesh, H., and Ehsani, M. R., *Prediction of failure load of R/C beams strengthened with FRP plate due to stress concentration at the plate end*, ACI Structural Journal, Vol. 95, No. 1, pp.142-152, January-February, 1998
12) El-Mihilmy, M., *Design and behavior of reinforced concrete beams strengthened with fiber-reinforced plastics (FRP)*, Ph.D. thesis, Auburn University, Alabama, USA, August, 1998
13) Wu, Z. S. and Niu, H. D., *Study on debonding failure load of RC beams strengthened with FRP sheets,* Journal of Structural Engineering, JSCE, Vol. 46A, pp.1431-1441, March, 2000
14) Wu, Z. S. and Niu, H. D., *Shear transfer along FRP-concrete interface in flexural members,* Journal of Materials, Concrete Structures and Pavements, JSCE, Vol. 49, No. 662, pp. 231-245, November, 2000
15) Triantafillou, T. C. and Plevris, N., *Strengthening of RC beams with epoxy-bonded fiber-composite materials,* Materials and Structures, pp.65-75, 1992
16) Kurokawa, T., Wu, Z. S. and Youshizawa, H., *Experimental investigation on crack characteristics of RC beams strengthened with CFRP plate*, Prpceedings of the 54th annual conference of the JSCE, Part 5, pp.702-703, 1999 (In Japanese)


(Received September 14, 2000)